

Two-dimensional mesoscopic Wigner crystallization and related issues

JEAN-LOUIS PICHARD

Service de Physique de l'Etat Condensé, CEA - Saclay, 91191 Gif sur Yvette Cedex, France

Abstract. The quantum-classical crossover from the Fermi liquid towards the Wigner solid is numerically revisited using small square lattice models where electrons interact via a Coulomb U/r potential. From exact numerical diagonalizations, one finds that the mesoscopic electron solid is formed in two stages, giving rise to an intriguing solid-liquid regime at intermediate couplings. The roles of a random substrate and of the spin degrees of freedom are investigated. Possible relations with the $2d$ metal-insulator transition observed in various field effect devices are suggested.

Keywords. Two-dimensional metal-insulator transition; Wigner crystallization.

PACS Nos 71.10-w; 71.27+a; 73.20.Qt

1. Introduction and lattice model

An outstanding question in quantum condensed matter is to know if the solid and the fluid can coexist in an intermediate phase separating the solid from the liquid. Such a phase was suggested [1] if the zero point motions of certain defects become sufficient to form waves propagating inside the solid. The statistics of the defects is given by the statistics of the particles out of which the solid is made. For bosons, they may form a condensate, giving rise to a superfluid coexisting with the solid. This supersolid phase is discussed in certain bosonic models [2]. For fermions, the defects may form a Fermi liquid [3] coexisting with the solid, such that the system is neither a solid nor a liquid. Two kinds of motion are possible in it; one possesses the properties of motion in an elastic solid, the second possesses the properties of motion in a liquid.

We study such a possibility in a mesoscopic system consisting of N electrons free to move on $L \times L$ square lattice with periodic boundary conditions (BCs). The Hamiltonian reads

$$\mathcal{H} = \sum_{i,\sigma} \left(-t \sum_{i'n.n.i} c_{i',\sigma}^\dagger c_{i,\sigma} + v_i n_{i,\sigma} \right) + \frac{U}{2} \sum_{\substack{i,i' \\ i \neq i'}} \frac{n_{i,\sigma} n_{i',\sigma'}}{|i-i'|} + 2U \sum_i n_{i,\uparrow} n_{i,\downarrow}, \quad (1)$$

where $c_{i,\sigma}$ ($c_{i,\sigma}^\dagger$) destroys (creates) an electron of spin σ at the site i and $n_{i,\sigma} = c_{i,\sigma}^\dagger c_{i,\sigma}$. The first terms describe the kinetic energy ($\propto -t$) and the random substrate energy (potentials v_i uniformly distributed inside $[-W/2, W/2]$). The interaction consists of a $U/|i-i'|$

Coulomb repulsion plus a $2U$ Hubbard repulsion. $|i - i'|$ is the smallest distance between the sites i and i' on a square lattice with periodic BCs. In our model, the Coulomb energy to kinetic energy ratio $r_s = U / (2t \sqrt{\pi n_e})$ for a filling factor $n_e = N/L^2$.

S and S_z are the total spin and its component along an arbitrary direction z . \mathcal{H} can be written in a block-diagonal form, with $N + 1$ blocks $\mathcal{H}(S_z)$ where $S_z = -N/2, \dots, N/2$ respectively.

2. Spinless fermions without disorder

Taking $N = 4$, $S_z = 2, 1, 0, -1, -2$ and since $\mathcal{H}(S_z) = \mathcal{H}(-S_z)$, one can restrict the study to the three blocks with $S_z \geq 0$. Taking $L = 6$, one can use Lanczos algorithm for diagonalizing the Hamiltonian and having the exact low eigenenergies $E_n(S_z)$ ($n = 0, 1, 2, \dots$). We first study [4] $\mathcal{H}(S_z = 2)$ (fully polarized electrons or spinless fermions) without a random substrate ($W = 0$). In this limit, the system remains invariant under rotation of angle $\pi/2$ and under translations and reflections along the longitudinal and transverse directions. Invariance under translations implies that the total momentum K is a good quantum number which remains unchanged when U varies. The symmetries imply that the states are fourfold degenerate if $K \neq 0$ and can be non-degenerate if $K = 0$.

Without interaction ($U = 0$), the states are $N_H = 58905$ plane wave Slater determinants (SDs) $\prod_{p=1}^4 d_{k(p)}^\dagger |0\rangle$, where $d_{k(p)}^\dagger$ creates a particle in a state of momentum $k(p) = 2\pi(p_x, p_y)/L$ and $|0\rangle$ is the vacuum state. The low energy eigenstates are:

- 4 degenerate ground states (GSs) $|K_0(\beta)\rangle$ of energy $E_0(U = 0) = -13t$;
- 25 first excitations of energy $E_1(U = 0) = -12t$;
- 64 second excitations $|K_2(\alpha)\rangle$ of energy $E_2(U = 0) = -11t$;
- 180 third excitations $|K_3(\alpha)\rangle$ of energy $E_3(U = 0) = -10t$;
- 384 fourth excitations of energy $E_4(U = 0) = -9t$.

Let us define 20 plane wave SDs useful to partly describe later the GS for intermediate ratios r_s . They are given by 4 plane wave SDs $|K_1(\beta)\rangle$ of energy $-12t$ where the particles have energies $-4t, -3t, -3t, -2t$ respectively, and by 16 plane waves SDs $|K_4(\delta)\rangle$ of energy $-9t$ where the particles have energies $-4t, -3t, -2t, 0t$ (first set of 8 SDs) and $-3t, -3t, -2t, -t$ (second set of 8 other SDs) respectively. Those 20 SDs of zero momenta ($K = \sum_{p=1}^4 k(p) = 0$) are directly coupled together by the pairwise interaction.

When one goes towards the classical limit ($t = 0$), the states become N_H Slater determinants $c_i^\dagger c_j^\dagger c_k^\dagger c_l^\dagger |0\rangle$ built out from the site orbitals. The low energy states are the following site SDs:

- 9 squares $|S_0(I)\rangle$ ($I = 1, \dots, 9$) of side $a = 3$ and of energy $E_0(t = 0) \approx 1.80U$;
- 36 parallelograms $|S_1(I)\rangle$ of sides $(3, \sqrt{10})$ and of energy $\approx 1.85U$;
- 36 other parallelograms $|S_2(I)\rangle$ of sides $(\sqrt{10}, \sqrt{10})$ and of energy $\approx 1.97U$;
- 144 deformed squares $|S_3(I)\rangle$ obtained by moving a single site of a square $|S_I\rangle$ by one lattice spacing and of energy $\approx 2U$.

For the first low energy states, the crossover from the $U = 0$ eigenbasis towards the $t = 0$ eigenbasis is shown in figure 1 (upper left) when one increases the ratio r_s . If we follow the 4 GSs $E_0(r_s = 0)$ (momentum $K_0 \neq 0$), one can see a first level crossing at $r_s^F \approx 9.3$ with a non-degenerate state of different momentum ($K_0 = 0$) which becomes the GS above r_s^F , followed by two other crossings with two other sets of 4 states with $K_l \neq 0$. When r_s is large, 9 states coming from $E_1(r_s = 0)$ have smaller energies than the 4 states coming from $E_0(r_s = 0)$. The degeneracies ordered by increasing energy become (1,4,4,4,...) instead of (4,25,64,...) for $r_s = 0$. These 9 low energy states give the 9

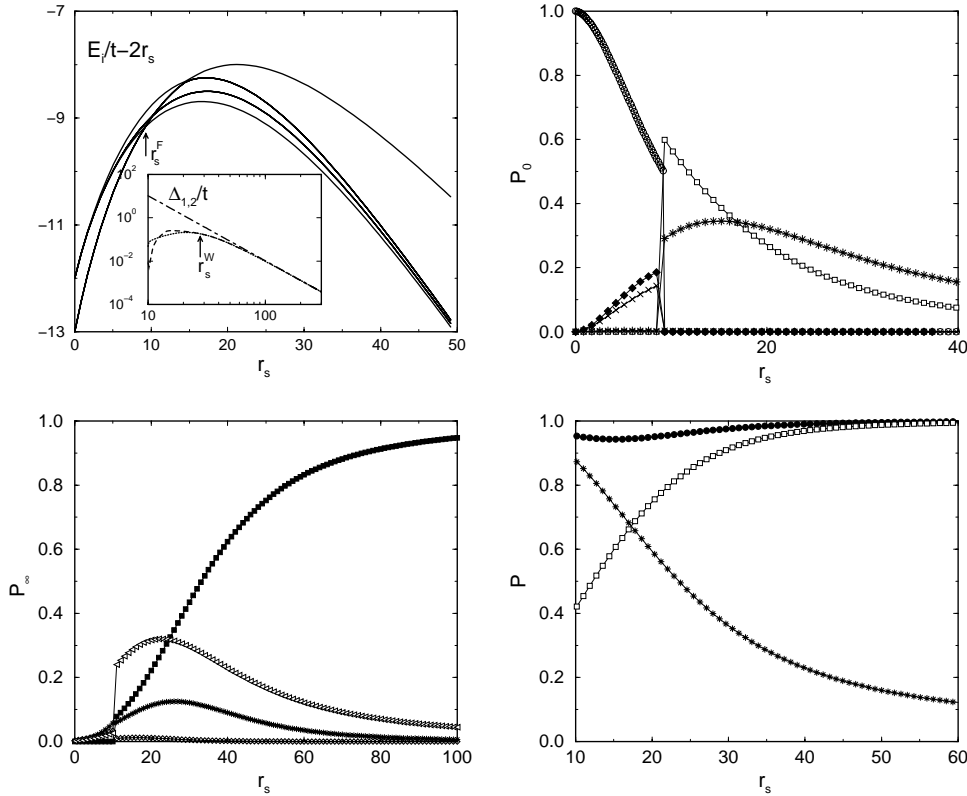


Figure 1. Upper left: Low energy part of the spectrum exhibiting a GS level crossing at r_s^F . Inset: two first level spacings Δ_1/t (dashed) and Δ_2/t (dotted) which become equal at r_s^W and the perturbative result $\Delta_1/t = \Delta_2/t \approx 10392/r_s^2$ valid when $r_s \rightarrow \infty$ (dot-dashed). Upper right: GS projections $P_0(r_s)$ onto a few plane wave SDs, given by the $4|K_0(\beta)\rangle$ (empty circle), the $4|K_1(\beta)\rangle$ (empty square), the $64|K_1(\alpha)\rangle$ (filled diamond), the $180|K_2(\alpha)\rangle$ (\times), the $16|K_4(\delta)\rangle$ (asterisk) respectively. Lower left: GS projection $P_s(r_s)$ onto a few site SDs, given by the 9 squares $|S_0(I)\rangle$ (filled square), the 36 parallelograms $|S_1(I)\rangle$ (asterisk), the 36 parallelograms $|S_2(I)\rangle$ (diamond), and the 144 deformed squares $|S_3(I)\rangle$ (left triangle) respectively. Lower right: GS projection $P'_0(r_s)$ (asterisk) and $P'_\infty(r_s)$ (empty square) and total GS projection P (filled circle) onto the re-orthonormalized basis using the low energy eigenvectors of the two limiting bases.

square molecules $|S_0(I)\rangle$ when $r_s \rightarrow \infty$. When r_s^{-1} is very small, they correspond to a solid square molecule free to move on a restricted 3×3 lattice, with an effective hopping term $T \propto tr_s^{-3}$ and a kinetic energy given by $-2T(\cos K_l(I) + \cos K_l(I))$ with $K_l(I) = 2\pi p_l/3$ and $K_l(I) = 2\pi p_l/3$ ($p_{l,t} = 1, 2, 3$). This structure with degeneracies 1, 4, 4 respectively and two equal energy spacings Δ_1 and Δ_2 appears (inset of figure 1 upper left) when r_s is larger than the crystallization threshold $r_s^W \approx 28$. The two characteristic thresholds r_s^F (level crossing) and r_s^W (9 first states having the structure of the spectrum of a single solid molecule free to move on a 3×3 square lattice) can also be detected by other methods which are discussed in ref. [4].

To understand further the nature of the intermediate GS between r_s^F and r_s^W , we have projected the GS wave functions $|\Psi_0(r_s)\rangle$ over the low energy eigenvectors of the two eigenbases valid for $U/t = 0$ and for $t/U = 0$ respectively. Let us begin with the $U = 0$ eigenbasis. Below r_s^F , each of the 4 GSs $|\Psi_0^\alpha(r_s)\rangle$ with $K_0 \neq 0$ still has a large projection $P_0(r_s, 0) = \sum_{\beta=1}^4 |\langle \Psi_0^\alpha(r_s) | K_0(\beta) \rangle|^2$ over the 4 non-interacting GSs. There is no projection over the 25 first excitations and smaller projections $P_0(r_s, 2)$ and $P_0(r_s, 3)$ over the 64 second and 180 third excitations of the non-interacting system. Above r_s^F , the non-degenerate GS with momentum $K_0 = 0$ has a large projection

$$P_0(r_s, 1) = \sum_{\beta=1}^4 |\langle \Psi_0(r_s) | K_1(\beta) \rangle|^2 \quad (2)$$

which is equally distributed over the 4 excitations $|K_1(\beta)\rangle$ of momentum $K_1 = 0$ and a second significant contribution

$$P_0(r_s, 4) = \sum_{\delta=1}^{16} |\langle \Psi_0(r_s) | K_4(\delta) \rangle|^2 \quad (3)$$

given by its projection onto the 16 mentioned plane wave SDs $|K_4(\delta)\rangle$ of energy $-9t$ and of zero momentum. Above r_s^F , its projections onto the 4 $|K_0(\beta)\rangle$, the 21 other first excitations and the second and third excitations of the non-interacting system are zero or extremely negligible. The total GS projection $P_0^t(r_s) = P_0(r_s, 1) + P_0(r_s, 4)$ onto the 4 $|K_1(\beta)\rangle$ and 16 $|K_4(\delta)\rangle$ is given in figure 1 (lower right) when $r_s > r_s^F$. This shows us that a large part of the system remains an excited liquid above r_s^F .

We now study the GS projections P_∞ onto the $t = 0$ eigenbasis. The GS projection

$$P_\infty(r_s, 0) = \sum_{I=1}^9 |\langle \Psi_0^\alpha(r_s) | S_0(I) \rangle|^2 \quad (4)$$

onto the 9 square site SDs $|S_0(I)\rangle$ is given in figure 1 (lower left), together with the GS projection $P_\infty(r_s, J)$ onto the site SDs corresponding to the J th degenerate low energy excitations of the $t = 0$ system. The total GS projection $P_\infty^t(r_s) = \sum_{p=0}^3 P_\infty(r_s, p)$ onto the 9 squares $|S_0(I)\rangle$, the 36 parallelograms $|S_1(I)\rangle$, the 36 other parallelograms $|S_2(I)\rangle$ and the 144 deformed squares $|S_3(I)\rangle$ is given in figure 1 (lower right) when $r_s > r_s^F$. The site SDs and plane wave SDs are not orthonormal. After re-orthonormalization, the total projection P of $|\Psi_0(r_s)\rangle$ over the subspace spanned by the 4 $|K_1(\beta)\rangle$ and 16 $|K_4(\delta)\rangle$ and 225 site SDs of lower electrostatic energies are given in figure 1 (lower right), showing that $|\Psi_0(r_s)\rangle$ is

almost entirely located inside this very small part of a huge Hilbert space for intermediate r_s , spanned by low energy SDs of different nature.

We conclude that for intermediate r_s , the ground state is a floppy solid entangled with an excited liquid of delocalized particles.

3. Spinless fermions with disorder

We now consider a statistical ensemble of clusters with $N = 4$ and $L = 6$ as before, but in the presence of a random substrate ($W = 5$). We still consider states with $S_z = 2$ (spinless fermions or fully polarized electrons), and study [5] the response to an Aharonov–Bohm flux ϕ which is enclosed along the longitudinal l -direction as sketched in figure 2. The BCs along the transverse t -direction remain periodic and the flux ϕ is included by taking appropriate longitudinal BCs. Antiperiodic BCs correspond to $\phi = \pi$ in our convention. The local persistent currents $\vec{J}(i)$ created at a site i are vectors defined by their longitudinal and transverse components ($\vec{J}(i) = (J_{i,l}, J_{i,t})$), or by their angles $\theta_i = \arctan(J_{i,t}/J_{i,l})$ and their absolute values $J_i = |\vec{J}_i|$. The longitudinal component $J_{i,l}$ of an eigenstate $|\Psi\rangle$ is defined as

$$J_{i,l} = 2\text{Im}\langle\Psi|c_{i_x+1,i_y}^\dagger c_{i_x,i_y} \exp(i\phi/L)|\Psi\rangle, \quad (5)$$

and $J_{i,t}$ is given by

$$J_{i,t} = 2\text{Im}\langle\Psi|c_{i_x,i_y+1}^\dagger c_{i_x,i_y}|\Psi\rangle. \quad (6)$$

The total current $I^{(n)}$ of the n th many-body wave function $|\Psi_n\rangle$ of energy E_n has a total longitudinal component $I_l(n)$ given by

$$I_l(n)(\bar{\phi}) = - \left. \frac{\partial E_n}{\partial \phi} \right|_{\phi=\bar{\phi}} = \frac{\sum_i J_{i,l}(n)}{L} \quad (7)$$

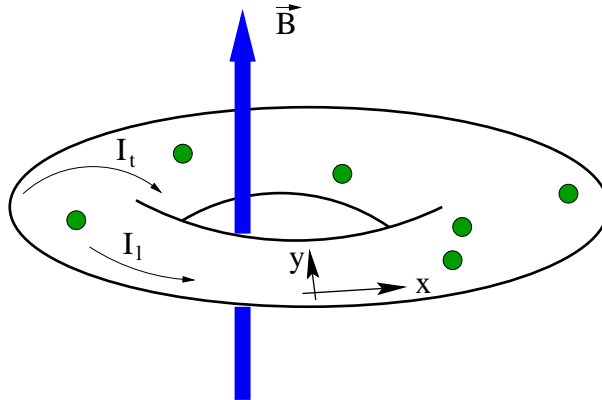


Figure 2. Two-dimensional torus with N electrons enclosing an Aharonov–Bohm flux $\phi = BL_x^2$.

which will be calculated for $\bar{\phi} = \pi/2$. As one increases U , a first characteristic threshold r_s^F can be identified by looking [5,6] at the average total longitudinal persistent current I_l of the GS at $\phi = \pi/2$, and comparing the exact quantity with the Hartree–Fock (HF) approximation. Below $r_s^F \approx 5$, the mean field approximation reproduces the exact I_l , but strongly underestimates I_l above r_s^F . This sharp breakdown of the HF approximation shown in figure 3 means that strong correlation effects occur above r_s^F , such that the shift of the GS energy when the BCs are changed cannot be obtained assuming the best possible SD for the ground state. One can also relate this breakdown of the HF approximation to the level crossing observed in the clean limit at $r_s^F \approx 9$, assuming that the level crossing of the clean system becomes a weakly avoided level crossing shifted to a lower value $r_s^F \approx 5$ in the presence of the random substrate, the disorder enhancing the interaction effect.

A closer investigation of the persistent currents of a typical sample gives three regimes, as shown in figures 4, 5 and 6. (see also ref. [7]). For weak coupling, the local currents flow randomly inside the cluster, due to elastic scattering on the site potentials. For intermediate coupling, the persistent currents remain important, but their pattern becomes oriented along the shortest direction enclosing ϕ . For large coupling, the oriented currents vanish. Reference [8] gives a detailed study of the large coupling limit where one can use perturbation theory for having the sign and the magnitude of I_l .

If one looks at the distribution of the angles θ_i of the local currents, one can see more precisely in figure 7 how the currents become aligned when one goes to the strong coupling limit. The ensemble average value $\langle |\theta| \rangle$ allows us to quantify the progressive change. If $p(\theta) = 1/(2\pi)$, $\langle |\theta| \rangle = \pi/2$, a value obtained for the low ratios r_s . At large r_s , $\langle |\theta| \rangle \rightarrow 0$. The ratio r_s at which the local currents cease to be oriented at random is consistent with the critical ratio r_s^F where the HF approximation breaks down.

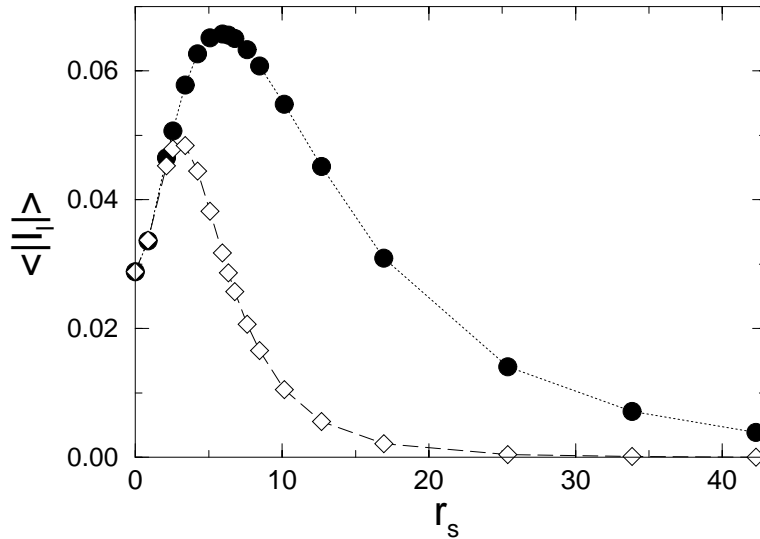


Figure 3. Ensemble average longitudinal GS current $\langle I_l \rangle$ as a function of r_s for $N = 4$, $L = 6$ and $W = 5$. Exact values (filled symbols) and values (empty symbols) obtained using the mean field Hartree–Fock approximation.

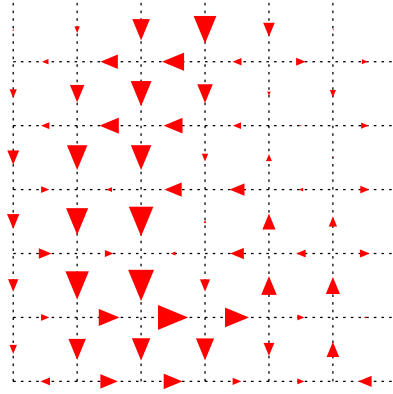


Figure 4. Map of the local persistent currents in a given sample for a small value of r_s .

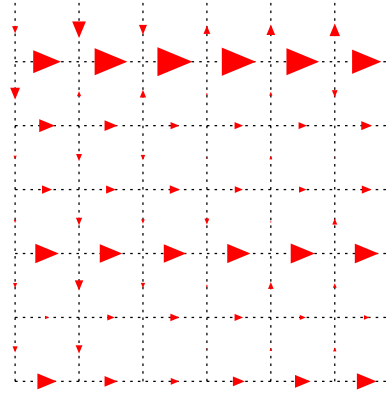


Figure 5. Map of the local persistent currents in a given sample for an intermediate value of r_s .

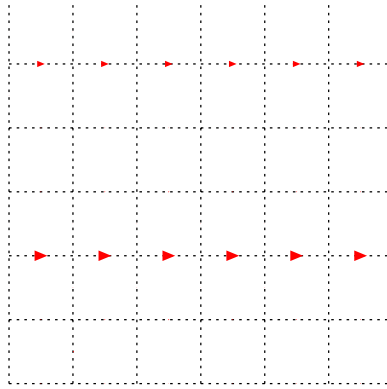


Figure 6. Map of the local persistent currents in a given sample for a large value of r_s .

Now, if one considers the average amplitude of the local currents, one can see in figure 8 that $\langle J_i \rangle$ is essentially independent of r_s up to a second threshold $r_s^W \approx 10$ which exceeds r_s^F . The crystallization parameter $\gamma = \max_r C(r) - \min_r C(r)$, where $C(r) = N^{-1} \sum_i \rho_i \rho_{i-r}$ and ρ_i is the electronic density at the site i , is defined in such a way that $\gamma = 1$ when the N particles form a rigid solid and 0 when they form a homogeneous liquid. Comparing in figure 8 the GS average crystallization parameter $\langle \gamma \rangle$ and $\langle J_i \rangle$, one can see that the suppression of the persistent currents coincides with the formation of a solid Wigner molecule.

In ref. [9], the low energy excitations of the same clusters have been studied, notably their statistics when the microscopic configurations of the random substrate are changed. For intermediate ratios r_s and with a random substrate, the 9 low energy states are characterized by oriented persistent currents and do not exhibit Wigner–Dyson (WD) spectral

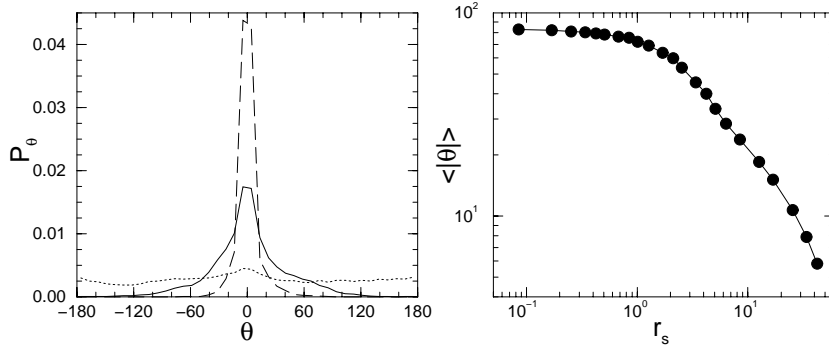


Figure 7. Left: Distribution P_θ of the GS local current angles for $r_s = 0$ (dotted line), $r_s = 6.3$ (full line) and $r_s = 42$ (dashed line). Right: Ensemble average angle $\langle |\theta| \rangle$ as a function of r_s .

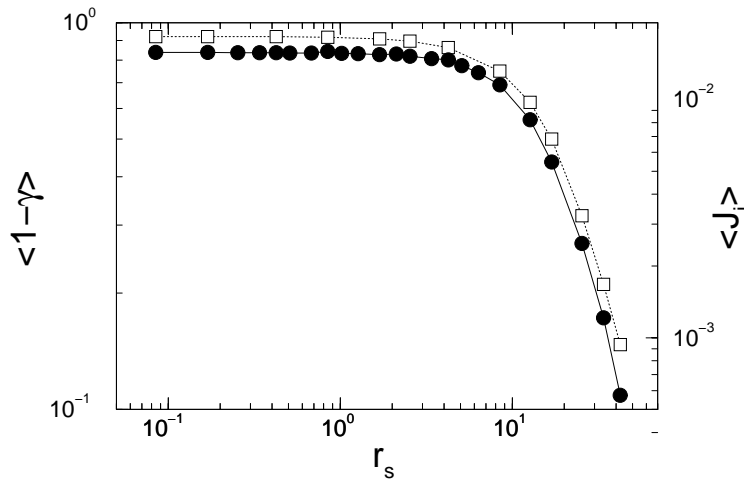


Figure 8. Averages of the GS crystallization parameter $\langle 1 - \gamma \rangle$ (left scale, empty symbols) and GS local current amplitude $\langle |J_i| \rangle$ (right scale, filled symbols) as a function of r_s .

statistics, while the local currents become randomly oriented and the levels obey WD statistics at higher excitation energies. Since the 9 first states correspond the 9 quantized modes of the kinetic energy of a rigid molecule in the clean limit and for large enough r_s , it is not surprising that a random substrate cannot make these 9 first states chaotic, in contrast to the higher energy states.

Firstly, one can conclude that the electron crystallization is favored by the random substrate: the intermediate correlated regime takes place for weaker values of r_s (typically $5 < r_s < 10$) than in the clean limit. Secondly, the intermediate regime is characterized by low energy levels able to support oriented persistent currents (in contrast to the Fermi limit)

which remain large (in contrast to the Wigner limit). The low energy spectral fluctuations give a third signature of the intermediate regime: WD statistics and randomly oriented local currents, if one excepts the 9 first states where the absence of WD statistics is accompanied by a non-random orientation of the local currents (see ref. [9]). This differs from the weak and strong coupling limits, where the spectral rigidity regularly decreases as the excitation energy increases.

4. Magnetization

We now consider the role of the spin degrees of freedom and of an applied parallel magnetic field B which aligns the spins without inducing orbital effects. For the previously studied ensemble of disordered clusters ($W = 5$, $N = 4$ and $L = 6$), we denote M the fraction of clusters with $S = 1$ at $B = 0$, $Q_2 = E_0(S_z = 2) - E_0(S_z = 0)$ and $Q_1 = E_0(S_z = 1) - E_0(S_z = 0)$ the Zeeman energies necessary to yield $S = 2$ and $S = 1$ respectively for a cluster with $S = 0$ when $B = 0$.

In figure 9, M is given as a function of r_s . One can see a first threshold at $r_s \approx 0.35$ where the interaction can drive $S = 1$ in certain samples. Above a second threshold r_s^{FS} , the fraction M ceases to increase and begins to regularly decrease to reach a zero value at a third threshold $r_s^{WS} \approx 9$ where an antiferromagnetic square molecule is formed. The ensemble averages $\langle \log Q_1 \rangle$ and $\langle \log Q_2 \rangle$ (without taking into account the $S = 1$ spontaneously magnetized clusters) define the typical fields B necessary to yield $S = 1$ or $S = 2$ in a $S = 0$

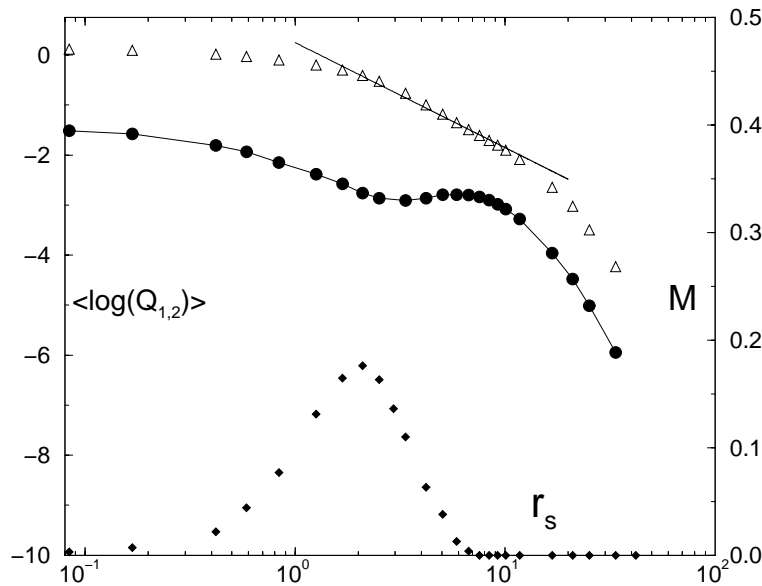


Figure 9. As a function of r_s , fraction M of clusters with $S = 1$ at $B = 0$ (filled diamond, right scale), partial $\langle \log Q_1 \rangle$ (filled circle, left scale) and total $\langle \log Q_2 \rangle$ (empty triangle, left scale) energies required to polarize $S = 0$ clusters to $S = 1$ and $S = 2$ respectively. The straight line corresponds to $0.25 - 2 \log r_s$. Statistical ensemble with $N = 4$, $L = 6$ and $W = 5$.

cluster. In figure 9, one can see an intermediate regime again for $r_s^{FS} < r_s < r_s^{WS}$ where $\langle \log Q_1 \rangle$ becomes roughly independent of r_s , while $Q_2 \propto r_s^{-2}$. As discussed in more detail in ref. [10], a signature of a specific intermediate regime is also given by the magnetization of mesoscopic clusters.

5. Conclusion and related issues

One concludes that mesoscopic Wigner crystallization proceeds in two stages, with or without a random substrate. The random substrate favors crystallization. A detailed GS analysis for a non-disordered cluster, the study for an ensemble of disordered clusters of the persistent currents driven by an Aharonov–Bohm flux, of the low energy spectral fluctuations and of the magnetization converge to the same conclusion: the existence of an intermediate regime where there is a floppy solid entangled with a liquid of delocalized electrons, and where a competition between the Stoner ferromagnetism and the Wigner antiferromagnetism takes place. In a clean system, a minimal description of the intermediate GS requires to combine the low energy states of the two limiting eigenbases, showing that the intermediate GS is neither solid, nor liquid, but rather the quantum superposition of those two states of matter, as proposed by Andreev and Lifshitz [1] long ago. It is interesting to compare our results obtained using a $2d$ torus with those obtained using $2d$ harmonic traps. Both the exact study of a two-electron artificial atom [11] and the Monte Carlo study [12] of a few electrons give a new intermediate regime where a ‘floppy’ molecule is observed. In ref. [12], this new regime corresponds to particles having a radial ordering on shells without correlated intershell rotation. One could think that this is due to the non-uniform particle density characterizing a harmonic trap. However, we find that the mesoscopic Wigner crystallization also takes place in two stages when the particles are confined on a $2d$ torus with a uniform density. Let us mention some physical problems for which these numerical results can be useful.

Firstly, the formation of a mesoscopic Wigner molecule is by itself an important issue which can be directly studied if one has a few electrons [13] confined in a quantum dot or a few ions [14] trapped by electric and magnetic fields. Increasing the size of the trap, a crossover from independent-particle towards collective motion can be observed.

Secondly, it becomes possible to create $2d$ gases of charges in high quality field effect devices and to vary by a gate the carrier density n_s such that the Coulomb energy to Fermi energy ratio $r_s \propto n_s^{-1/2}$ can reach high values where the charges become strongly correlated. Doped semi-conductors [15] (Si–Mosfet, Ga–As heterostructures, Si–Ge quantum wells) or undoped organic crystals [16] can be used. Since charged crystallization is expected for $r_s \approx 37$ in a clean system [17] and at lower r_s in the presence of impurities [5,18], to study how one goes in two dimensions from a Fermi liquid (low r_s) towards a Wigner crystal (large r_s) becomes possible. Transport measurements [15] performed in macroscopic samples indicate an unexpected low temperature metallic behavior for intermediate values of r_s which raise the question of the existence of a possible intermediate phase, which should be neither a Fermi system of localized particles (Anderson insulator), nor a correlated and rigid solid of charges (pinned insulating Wigner crystal). One can also mention that a microscopic restructuring of the charges is seen using local compressibility measurements at the two-dimensional metal–insulator transition, the system being more homogeneous in the intermediate metallic phase than in the low density insulating limit [19,20].

Having in mind these experimental observations, one can conclude by stressing the interest to study if this crystallization in two stages persists when one goes from the mesoscopic limit towards the macroscopic limit, and how charge transport takes place for intermediate couplings.

Acknowledgements

My own research on this subject (for a more extended review, see ref. [6]) was published in a series of letters [4,5,9,10] done with G Benenti, G Katomeris, F Selva and X Waintal. I acknowledge with thanks these fruitful collaborations.

References

- [1] A F Andreev and I M Lifshitz, *Sov. Phys. JETP* **29**, 1107 (1969)
- [2] G G Batrouni and R T Scalettar, *Phys. Rev. Lett.* **84**, 1599 (2000)
- [3] I E Dzyaloshinskii, P S Kondratenko and V S Levchenkov, *Sov. Phys. JETP* **35**, 823 (1972); **35**, 1213 (1972)
- [4] G Katomeris and J-L Pichard, cond-mat/0012213
- [5] G Benenti, X Waintal and J-L Pichard, *Phys. Rev. Lett.* **83**, 1826 (1999)
- [6] J-L Pichard, G Benenti, G Katomeris, F Selva and X Waintal, in *Exotic states in quantum nanostructures* edited by S Sarker (Kluwer Academic Publishers) cond-mat/0107380
- [7] R Berkovits and Y Avishai, *Phys. Rev.* **B57**, R15076 (1998)
- [8] F Selva and D Weinmann, *Europhys. J.* **B18**, 137 (2000)
- [9] G Benenti, X Waintal and J-L Pichard, *Europhys. Lett.* **51**, 89 (2000)
- [10] F Selva and J-L Pichard, *Europhys. Lett.* **55**, 518 (2001)
- [11] C Yannouleas and U Landman, *Phys. Rev. Lett.* **85**, 1726 (2000)
- [12] A V Filinov, M Bonitz and Yu E Lozovik, *Phys. Rev. Lett.* **86**, 3851 (2001)
- [13] R C Ashoori, *Nature* **379**, 413 (1996)
- [14] D H Dubin and T M O'Neil, *Rev. Mod. Phys.* **71**, 87 (1999)
- [15] E Abrahams, S V Kravchenko and M P Sarachik, *Rev. Mod. Phys.* **73**, 251 (2001) and references therein
- [16] J H Schön, S Berg, Ch Kloc and B Batlogg, *Science* **287**, 1022 (2000)
- [17] B Tanatar and D M Ceperley, *Phys. Rev.* **B39**, 5005 (1989)
- [18] S T Chui and B Tanatar, *Phys. Rev. Lett.* **74**, 458 (1995)
- [19] S Ilani, A Yacoby, D Mahalu and Hadas Shtrikman, *Phys. Rev. Lett.* **84**, 3133 (2000)
- [20] S Ilani, A Yacoby, D Mahalu and Hadas Shtrikman, *Science* **292**, 1354 (2001)